Ion Acoustic Wave Propagation and Heating in a High-Current Hollow Cathode Plume

IEPC-2017-398

Presented at the 35th International Electric Propulsion Conference
Georgia Institute of Technology – Atlanta, Georgia – USA
October 8–12, 2017

Christopher A. Dodson*
University of California, Los Angeles, CA, U.S.A.

Benjamin A. Jorns†
University of Michigan, Ann Arbor, MI, U.S.A.

Richard E. Wirz‡
University of California, Los Angeles, CA, U.S.A.

High current hollow cathodes used for electric propulsion have been found to have energetic ions in the plume caused by a mechanism still not fully understood. These anomalously energetic ions have been shown to erode cathode keepers and pose a risk to cathodes used for long-duration missions. This work builds on previous work investigating the effects of ion acoustic turbulence (IAT) in the plume and its effects on the ion population. Laser-induced fluorescence (LIF) and plasma probes were used to measure several steady-state and fluctuating plasma properties related to ion acoustic waves. A preliminary analysis of these data show the ion distribution function along the the centerline to be heated primarily in the axial direction resulting in ion temperature anisotropy. A bimodal ion velocity distribution function was observed with the axial LIF beam near the anode, consisting of slow and fast populations. It was not possible to detect two distinct populations using the radial LIF measurements. The fast population was found to accelerate with distance from the keeper orifice whereas the slow ion population remained nearly stationary, and is believed to be caused by ion generation in the plume through ionization or charge-exchange collisions. Wave energy and the ion acoustic wave direction were measured and show an increase in wave energy downstream, highly concentrated along the centerline. The ion acoustic waves were found to propagate outward from the orifice and are approximately collinear with the drift direction of the fast ion population.

*Ph.D. Candidate, Aerospace Engineering
†Assistant Professor, Department of Aerospace Engineering
‡Associate Professor, Mechanical and Aerospace Engineering

Nomenclature

A	=	amplitude of oscillation
k	=	Wavenumber
f	=	Laser frequency
c	=	Speed of light
k_B	=	Boltzmann's constant
A	=	Area, m^2
m	=	Mass, kg
I	=	Current, A
γ	=	Wave growth rate
ω	=	Angular frequency [rad/s]
W	=	Energy
v	=	Velocity
ϕ	=	Potential
c_s	=	Ion acoustic speed
ν	=	Frequency [Hz]
$f(v)$	=	Velocity distribution function
V	=	Drift velocity
q	=	Fundamental charge
n_s	=	Density
T_s	=	Temperature
z	=	Axial distance
r	=	Radial distance

I. Introduction

Long-duration space missions using electric propulsion typically use hollow cathodes for ionization and neutralization. Proposed missions are now exceeding 50 kh of cathode operation, so to reduce development cost and duration, cathode plume models are increasingly being relied upon for lifetime prediction. Two aspects of hollow cathode plume physics not fully understood include anomalous resistivity and energetic ion production. The former has shown to be related to scattering of electrons off of electric field fluctuations caused by ion acoustic turbulence (IAT),[1] resulting in the anomalously high plasma potential measured in the near field of the plume. The latter issue is the motivation of this work, which seeks to provide experimental measurements of near plume plasma properties to better understand mechanisms that could cause ions to exceed energies possible due to electrostatic acceleration or pressure gradients.

Energetic ion production was first observed during high current cathode experiments in ion thruster discharges in the late 1980's, and have since been characterized by many authors. Several mechanisms have been proposed for their formation, one of which is IAT. Recent work at JPL has shown a correlation between IAT wave energy and ion temperature along the centerline for several operating conditions.[2] In regions where the IAT had fully developed this correlation was on the order of that predicted by Jorns.[3] This work expands upon the research in Refs. 2 and 4 by presenting measurements of axial and radial ion velocity distribution functions (IVDF's) using laser-induced fluorescence (LIF). Additionally, the wave energy propagation direction was measured using an array of ion saturation probes. The findings are presented as follows. In Sec. II the basics of ion acoustic turbulence is discussed. Section III covers the experimental diagnostics used. Section IV presents preliminary results of the experimental campaign along with discussion.

II. Ion Acoustic Turbulence Theory

A. Ion Acoustic Waves and Turbulence

Ion acoustic waves are produced when the velocity of the electrons in the reference frame of the ions exceeds the ion acoustic speed,[5] $c_s = \sqrt{(T_e + \gamma_i T_i)/m_i}$, where T_e and T_i are the electron and ion temperatures, respectively, in eV, m_i is ion mass, $\gamma_i = 3$ (corresponding to longitudinal compressions), the electrons are assumed to be isothermal, and it is assumed that Landau damping from ions is small. These waves are unstable and develop into IAT which exchanges momentum with the ions and electrons. The source of free energy in IAT is the relative drift velocity of the electrons relative to the ions, and energy is transferred to the wave through inverse electron Landau damping. Scattering of the electrons on the waves results in anomalous resistivity (in that it can greatly exceed the classical resistivity caused by Coulomb collisions) and Joule heating of the electron population. The ions interact with the waves through ion Landau damping, which extracts energy from the waves to heat the ions. The turbulent waves exist as a cone-shaped spectrum of vectors pointing in the direction of the relative electron drift velocity.[5] In the following we ignore the oblique components of the waves since maximum growth is in the direction of the relative drift between the electrons and ions, $\vec{V}_e - \vec{V}_i$.

The dispersion relation for ion acoustic waves along the centerline of a cathode plume is given in Ref. 6. The real part of the dispersion relation, which is what is measured in this experiment, is given by:

$$\omega_R = k(c_s + V_i), \tag{1}$$

where ω is wave frequency and k is wavenumber. It is assumed that the wavelength is long compared to the Debye length and that the plasma is uniform locally (i.e. it varies slowly compared to the wavelength of the wave).

III. Experimental Setup

The experiments were performed in a 2.6 m x 5.2 m long vacuum chamber facility at JPL with a pumping speed of ∼40 kL/s and a base pressure of $\sim 10^{-7}$ Torr. The cathode discharge was powered by a 330 A Sorensen power supply. Cathode flow control was provided by an Apex flow controller, and research grade xenon gas was used for all testing. The cathode used for these experiments was designed for 100 A and had a LaB_6 insert material, and is shown in Fig. 1(a). The cathode tube and keeper were made of graphite and the orifice plate was made of tungsten. The anode consisted of a 100 mm diameter, 300 mm long, cylindrical copper tube that was located 30 mm downstream of the keeper. It was concentrically aligned with the cathode and water cooled. The inside of the anode was lined with tungsten sheets to prevent sputtered copper from the anode from depositing onto the cathode (since tungsten has a lower sputter yield than copper). The cathode assembly was mounted to two stages that provided axial and lateral translation of the assembly, while probe and optical diagnostics remained fixed, as shown in Fig. 1(b). The cathode was kept at ground potential, and the anode was biased relative to cathode. No magnetic field was applied to the plume region to minimize the number of modes present and simplify interpretation of probe measurements.

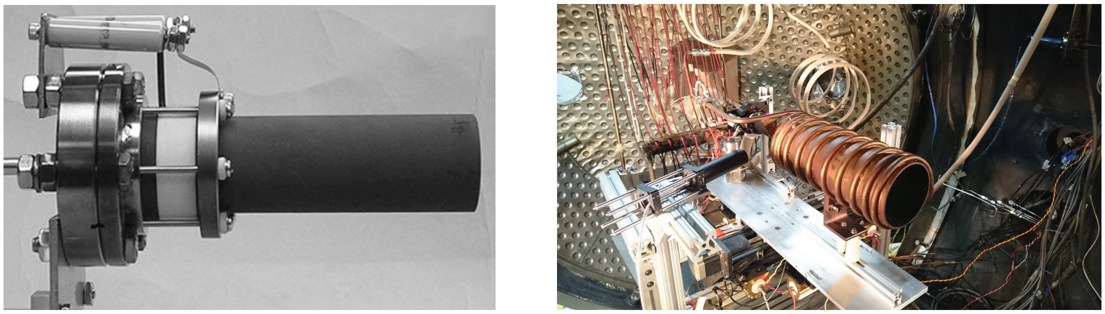

(a) 100 A, 1/2" LaB_6 Hollow Cathode (b) Cathode assembly and test configuration.

Figure 1. Cathode assembly.

A. Steady State Langmuir Probe Measurements

An array of cylindrical Langmuir probes (Fig. 2) was used for all probe measurements. For steady-state measurements of plasma density, electron temperature, and plasma potential, only the corner probe of the array was used and the other two probes were allowed to float. The measurement domain domain was sampled with Δr=3 mm and Δz=2 mm. This section will describe the interpretation of the Langmuir probe measurements.

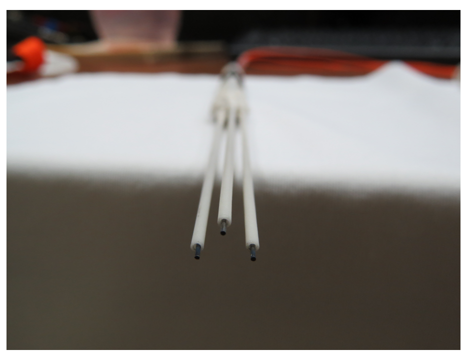

Figure 2. Langmuir probe array. The separation between orthogonal pairs is ~5 mm.

1. Density

Biasing the probe sufficiently negative to repel a majority of the electrons allows the ion saturation current to be measured which can be related to the background plasma density. Traditional Langmuir probe analysis neglects ion drift and finite ion temperature. The Bohm sheath criterion states that the ions enter the sheath at the ion acoustic speed, $c_s = \sqrt{(T_e + \gamma_i T_i / m_i}$, where $\gamma_i = 3$ since the ion density compressions are assumed to be one-dimensional. Under these assumptions, the ratio of ion density at the sheath boundary to the bulk plasma is $e^{-1/2}$ using the Boltzmann relation for electrons. The plasma density measurement from ion saturation current is then given by $n_0 = I_{sat}/e^{-1/2} q A c_s$, where I_{sat} is the ion saturation current, q is the fundamental charge, and A is the collection area of the sheath. In the cathode plume the ratio of the probe radius to the Debye length, $r_p/\lambda_{De} \sim 300$, allowing the use of the thin-sheath approximation[7] where the sheath area is assumed to be equal to the probe area.

The approach outlined here, and the results presented in Sec. IV, assumes ion drifts are small relative to their thermal speeds (i.e. $M_i, M_e \ll 1$), where M_s is the Mach number. However, centerline Mach numbers of 2-4 for ions[2] have been measured, indicating that drift effects on density measurements may be important. An estimate for this effect can be performed based on the results of McMahon,[8] who performed simulations of drifting plasmas incident on cylindrical probes. The result is that calculations for non-drifting ions tend to overestimate plasma density by a factor of 2 along the plume centerline compared to drifting plasmas, assuming ion temperature isotropy and a constant ratio of ion to electron temperature. However, as will be shown in the Results section, ion temperature anisotropy, electron temperature, and plasma potential are all varying throughout the plume. Because proper correction for flowing effects on density are outside the scope of this paper, the results in Sec. IV should be viewed with the understanding that the corrected densities could be lower than that shown.

2. Electron Temperature

The electron temperature was inferred from an exponential fit to the electron current-voltage trace[7] calculated assuming a linear fit to the ion saturation current portion, resulting in $T_e = \phi_{bias}/\ln(I_e)$. However, this approach ignores the electron drift which, for a drifting Maxwellian electron population incident on a probe, can result in a significant modification to the equation used for estimating T_e if $M_e = V_e/v_{e,th} > 0.1$.[9] For a cylindrical probe oriented with the probe axis orthogonal to the electron drift direction the traditional analysis tends to overestimate T_e, and this correction factor scales with the drift magnitude as $T_{e,drifting}/T_{e,stationary} = e^{1.12M_e}$. Applying this correction and using the Mach numbers calculated by Jorns for this operating condition in Ref. 4 (where $M_e \sim 1-2$), the electron temperatures would be reduced by a factor of 2-9.

The challenge in applying this correction is knowing the electron drift velocity. The approach by Jorns[4] estimates the average electron drift by integrating the electron current density over an area at a fixed axial position with a known total current., but this is valid only along the centerline and could be underestimating the max drift due to averaging. Because it was not possible to measure or estimate the electron drift off-axis, in this paper T_e is calculated assuming a non-drifting Maxwellian electron population, with the understanding that this approach may result in an overestimate of T_e in regions of significant electron drift.

3. Plasma Potential

It was found that biasing the probe >10 V resulted in excessively high electron current and the probe became emissive. This prevented electron current measurements near the electron saturation region of the I-V curve, so it was not possible to determine plasma potential using the knee of the characteristic. Because of this, plasma potential was approximated by equating the electron saturation current for slow, Maxwellian electrons with the ion current for slow, isotropic ions entering the sheath at the Bohm velocity $v_{Bohm} = \sqrt{T_e/m_i}$, resulting in the following relationship:[7]

$$\phi_p = \phi_f - T_e \ln\left[\alpha\sqrt{\frac{2\pi m_e}{m_i}}\right], \tag{2}$$

where ϕ_p is the plasma potential and ϕ_f is the floating potential. Note that the previous discussion of the effects of drifts illustrate the significant uncertainty (not quantified here) inherent in this estimate of plasma potential. Nevertheless, this treatment was used to show the qualitative structure of the plasma potential.

B. Fluctuation Measurements

1. Wave Energy Density

The total wave energy, using the dispersion relation of ion acoustic waves subject to the simplifying assumptions above, yields the following results for the energy of electrostatic waves:[10]

$$E_T = \sum_k \frac{q^2\widetilde{\phi}_k^2}{T_e(1+3T_i/T_e)}\left[1+\frac{V_i}{c_s}\right], \tag{3}$$

where $\widetilde{\phi}_k$ is the amplitude of the fluctuating plasma potential of acoustic mode with wavenumber k and q is the fundamental charge. The potential amplitude spectrum can be measured using the cylindrical Langmuir probe array discussed earlier by applying a negative bias voltage of -27 V and measuring the voltage drop across a shunt resistor. The bias was applied using a set of batteries connected to ground to avoid any low-impedance paths to ground that could exist in a power supply, which would affect high frequency measurements. Fluctuation measurements used for wave energy calculations were only taken on the upstream probe to avoid any potential wake effects due to particle flow.

To obtain the fluctuating plasma potential power spectrum, $\widetilde{\phi}$, the following relationship holds for electrostatic perturbations of small amplitude:

$$\widetilde{\phi} = \frac{k_B T_e}{q}\left(\frac{\widetilde{n}_i}{\overline{n}_i}\right). \tag{4}$$

where $\widetilde{n}_i/\overline{n}_i = \widetilde{I}_{sat}/\overline{I}_{sat}$. Note that this treatment does not account for electron or ion drifts, which we have shown to be important for density and electron temperature calculations. Neglecting ion drift is justified in this derivation because Eq. 3 accounts for the Doppler shift of the wave frequency.

2. Wave Dispersion

The signals on a pair of fixed probes can be analyzed to determine the dispersion relation, $k(\omega)$, by using the cross-phase of ion saturation current signals from two probes using the approach by Beall,[11] which is only briefly described here. For any two signals, the dispersion relation between them can be determined by taking the Fourier transform $\mathcal{F}$ of each and using the following relationship:

$$k(\omega) = \frac{1}{\Delta x} tan^{-1}\left[\frac{\mathrm{Im}(\mathcal{F}[\phi_2(t)]\mathcal{F}^*[\phi_1(t)])}{\mathrm{Re}(\mathcal{F}[\phi_2(t)]\mathcal{F}^*[\phi_1(t)])}\right]. \tag{5}$$

where Δx is the probe separation distance, and the fluctuations in plasma potential are represented in the Eikonal approximation as $\phi(t) = \sum_\omega \phi(\omega)e^{i[k(\omega)x-\omega t]}$. To improve the correlation with noisy signals, the Beall approach involves averaging over a number of time signals using a histogram technique, binning the k values and weighting them according to the following:

$$S(\omega, k) = \frac{1}{M}\sum_{j=1}^{M} I_{0,\Delta k}[k - k^j(\omega)]\frac{1}{2}[P_1^{(j)}(\omega) + P_2^{(j)}(\omega)], \tag{6}$$

where M is the number of time samples, j is the run number, $P_1^{(j)}$ and $P_2^{(j)}$ are the power spectra of the two signals. The function $I(x)$ is used to ignore wavenumbers not discernible based on the probe separation distance, and is defined as

$$I_{0,\Delta k}(x) = \begin{cases} 1, & |k - k^j(\omega)| < \Delta k \\ 0, & |k - k^j(\omega)| > \Delta k. \end{cases} \tag{7}$$

where Δk is the width of the bin. Performing this analysis on both sets of probes, oriented parallel and perpendicular to the cathode axis, gives the dispersion relation in each direction. The phase velocity ($v_{ph} = \omega/k$)in the axial and radial directions are obtained from the slope of the dispersion relations. The wave propagation direction is then obtained from the vector sum of the component phase velocities. For the results shown here, the wave vectors were determined by manually identifying the portion of the dispersion relation in which the dispersion relation was linear to obtain the slope. To verify that the plasma wake from the upstream probe did not affect the fluctuation measurements of the downstream probe, the ion saturation currents were compared along the centerline. It was found that the downstream probe measurement was within 5% of the upstream probe for $z \geq 5$ mm, indicating that the wake of the upstream probe did not affect at least the steady-state density measurements. An example of the axial dispersion plot obtained using the Beall techniques is shown in Fig. 3, illustrating the linear dispersion characteristic of ion acoustic waves.

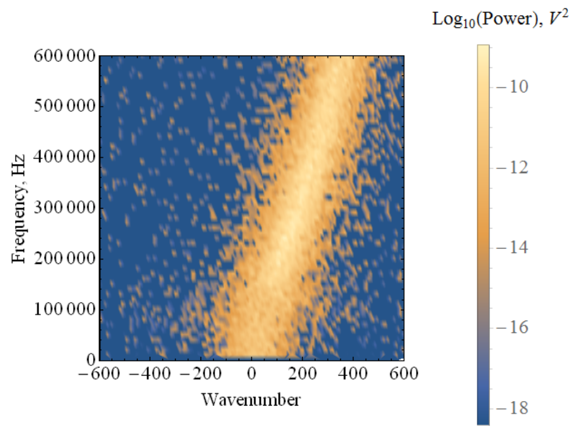

Figure 3. Example Beall plot for axial dispersion.

C. Laser-Induced Fluorescence

LIF was used to measure the local evolution of the IVDF in the near field plume. This technique involves measurinng the Doppler shift of an absorption line of singly-ionized xenon, using the relationship $v_i = c\Delta f/f_0$, where v_i is ion velocity, Δf is the difference between the laser frequency and the frequency of the absorption transition in the rest frame of the ions, f_0, and c is the speed of light. Due to its high transition probability and accessibility using diode lasers, the XeII $5d^2F_{7/2} \rightarrow 6d_2^{5/2}$ transition was excited using 834.953 nm (vacuum), resulting in fluorescence at 542.066 nm (vacuum).[12,13] A 500 mW CW diode laser (Fig. 4(a)) was coupled to the vacuum chamber via multimode fibers and focused to a spot size of ∼2 mm to either an axially- or radially-oriented injection optical assembly, fixed relative to the cathode (Fig. 4(b)). A maximum of 130 mW average laser power was used to maximize signal-to-noise for the wings of the plume and near the keeper, where the low density made it challenging to resolve the IVDF. The spot size of the collection optics was ∼1.2 mm, and the fluorescence light was fiber-coupled to a photomultiplier tube located outside of the chamber. A bandpass filter centered at 543 nm was used to isolate the fluorescence signal from other emission lines. A current amplifier and lock-in amplifier were used along with an optical chopper for phase-sensitive detection. Measurements of axial IVDF's were taken independently of radial IVDF's to maximize signal strength. Because there was no applied magnetic field, Zeeman splitting was assumed to be negligible in the plume, eliminating the need for polarizers on the injection beams.

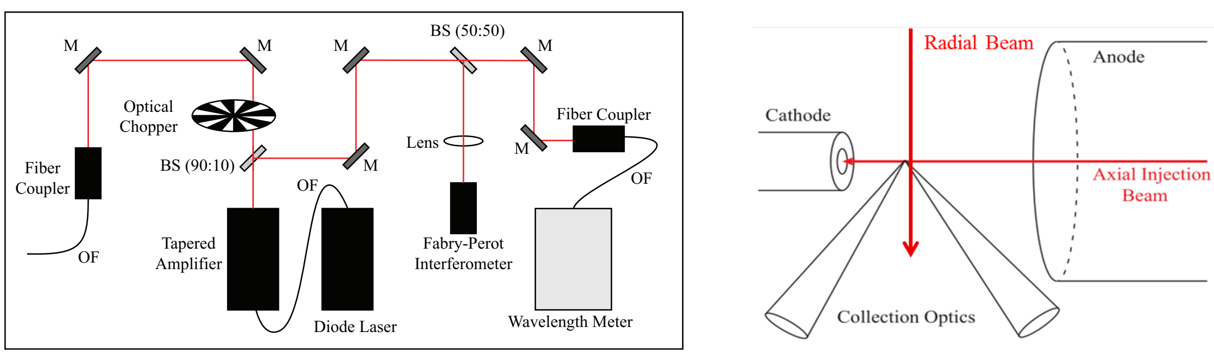

(a) Optical bench (M: mirror, BS: beam splitter, OF: optical fiber).

(b) Chamber configuration.

Figure 4. Laser-induced fluorescence (LIF) system.

IV. Experimental Results and Discussion

The results of this preliminary analysis were for the 160 A, 15 sccm operating condition with a background pressure of 1x10^{-5} Torr. The cathode discharge voltage was ∼23 V. First the background plasma properties will be discussed that are needed to calculate the ion acoustic wave energy, followd by presentation of the LIF and wave measurements.

A. Background Plasma Properties

Figure 5 shows the calculated plasma density, electron temperature, and plasma potential in the plume. The contour plots were generated using first order interpolation. The density shows a nearly collimated shape within the keeper radius (5 mm). Electron temperatures of 2.5-3.5 eV are found throughout the majority of the measurement domain but dropping significantly at the wings. The plasma potential shows a potential trough caused by the large electron current in the main jet, with increasing potential towards the wings of the plume. Along the centerline the potential gradient is negligible. Note also that the calculated plasma potential near the wings exceeds that of the discharge voltage, indicating an error in this method of estimating potential using the floating potential and electron temperature. It could also be due to electron temperature uncertainty on the wings where the signal-to-noise ratio was poor. Since the steady-state plasma potential measured using the Langmuir probe sweeps was not used for either ion or wave calculations, Fig. 5(c) is presented only to show the qualitative behavior in the plume.

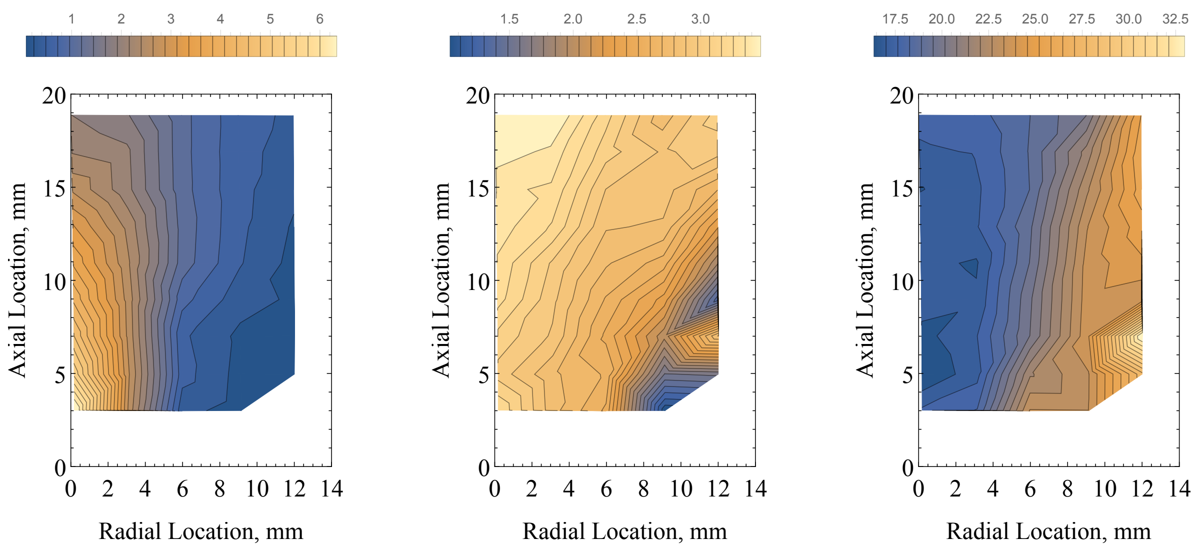

(a) Plasma density (x10$^{19}m^{-3}$).

(b) Electron temperature (eV).

(c) Plasma potential (V).

Figure 5. Plasma properties for the 130 A, 15 sccm, 1x10^{-5} Torr background pressure operating condition.

B. LIF Measurements

The ion properties in the plume discussed here were obtained using LIF. A retarding potential analyzer (RPA) was used to obtain ion energy distribution function measurements along the centerline and in the radial directions in the far plume as a check on the LIF results. Since past experiments[2] have shown the LIF results to approximately converge to the RPA values in the far plume, the RPA results are not presented here. The domain was sampled with Δr=3 mm and Δz=4 mm. Figure 6 shows several of the axial IVDF's measured throughout the domain, along with the curve fit applied to the drifting component (in red). The axial and radial locations are indicated in the upper corner of each box, respectively. The radial IVDF profiles are not shown because they all could be fit by single Gaussian curve fits and showed no unexpected peaks.

Several features can be seen in the axial IVDF plots worth discussing here. First, for regions outside the cathode orifice but near the keeper (i.e. for r≥3 mm and z≤11 mm) a second, negative velocity peak was observed, with velocity opposite that of the positive-going peak but with varying amplitude. This is believed to be due to reflection of the axial LIF injection beam off the tungsten orifice and off of tungsten deposition on the keeper face, caused from sputtering of the anode liner, which was found to be significant in the post-test examination of the keeper. Additionally, for regions farther into the plume (z>11 mm) a second peak in the signal is found approximately centered at 0 km/s, and will be referred to here as the slow population. To differentiate between the fast and slow populations, and between real and artificial populations in the regions with laser reflections, a dual Gaussian distribution was used to fit the two peaks:

$$f_i(v) = n_{01}\sqrt{\frac{m_i}{2\pi T_{i1}}}e^{-\frac{m_i(v-V_{01})^2}{2T_{i1}}} + n_{02}\sqrt{\frac{m_i}{2\pi T_{i2}}}e^{-\frac{m_i(v-V_{02})^2}{2T_{i2}}}, \tag{8}$$

where subscripts V_{01} and V_{02} denote the most probable velocity of the slow and fast populations. One possible explanation for the slow population is the generation of ions in the plume from electron-bombardment or charge-exchange collisions, both of which have mean free paths on the order of the cathode-anode separation distance. However, since ionization and charge-exchange are isotropic, slow peaks would be expected in the radial IVDF's but none were observed. However, it is possible that the radial velocity distribution functions of the two populations were closely overlapped in velocity space. Reflections of fluorescence light off of the tungsten liner was also ruled out as a potential cause of the slow peak by measuring the IVDF using collection optics oriented such that the view path did not intersect the reflective anode tungsten liner. This bimodal IVDF could affect the IAT energy balance as well as the interpretation of Langmuir probe data so should be considered in future analysis of plume measurements.

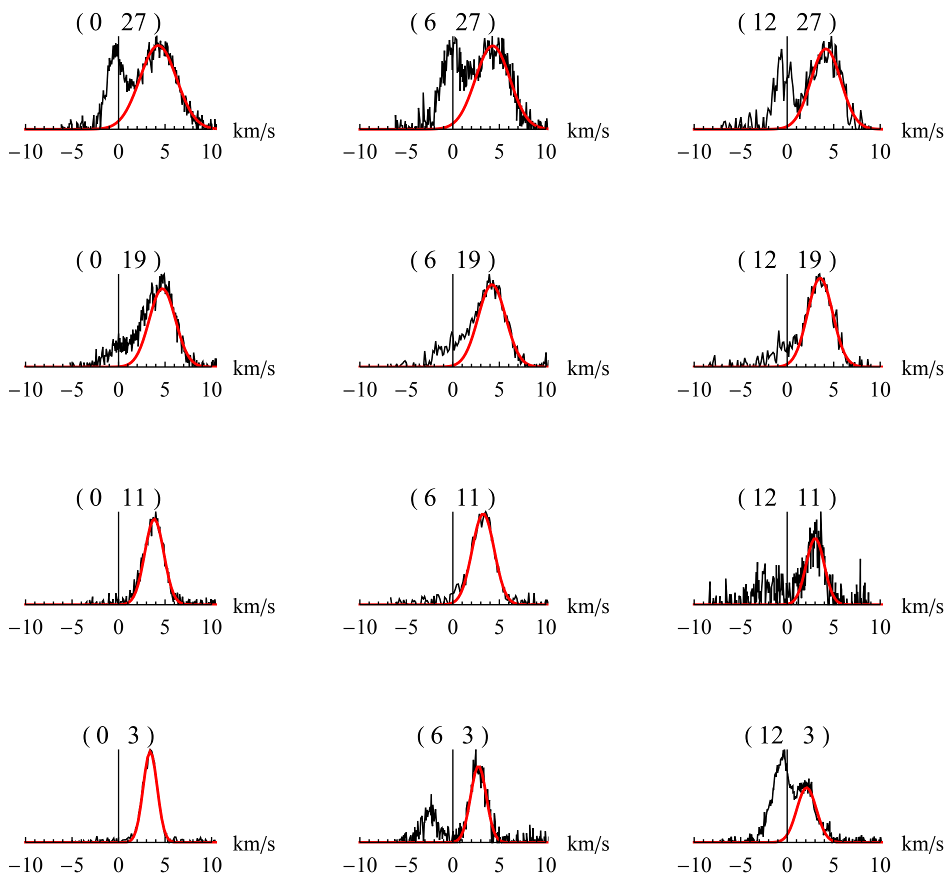

Figure 6. Axial IVDF's measured by LIF. The raw data is shown in black and the Gaussian fit to the fast population is shown in red. The (z,r) coordinates in *mm* are indicated above each plot.

The results of for ion drift direction and magnitude for the fast population are shown in Figure 7(a), using first order interpolation for the drift magnitude contour plot. The vectors are normalized to the net drift speed. Both the axial and radial drift components increase with distance from the cathode orifice, beginning at ~2.5 km/s and increasing to nearly 5 km/s near the anode. The cause of this acceleration is planned to be investigated further.

Figure 7(b) shows a representation of the variances of the Gaussian fits to the IVDF chords measured using the axial and radial injection beams. The origin corresponds to the keeper orifice center, which shows a nearly isotropic distribution with ~1 eV for both IVDF measurements. The length of the bars represents temperature and the bars are aligned with the direction of the injected beam. Both the axial and radial IVDF's obtained show an increase in the temperature with distance from the cathode orifice. Along the centerline the ions start out isotropic with T_i=1 eV, and evolve downstream to have an axial temperature of ~5 eV with the radial temperature only increasing slightly. One proposed mechanism for the increasing ion temperature is IAT, as discussed in Refs. 2, 3. Analysis of the fluorescence response as a function of laser intensity, along with calculations assuming a simplified two-level energy level model (neglecting hyperfine splitting), indicates a moderate amount of saturation which could have broadened the IVDF by 10-20%.[14] Experiments at UCLA are planned to more accurately quantify the degree of saturation present and the uncertainty in the temperature measurements.

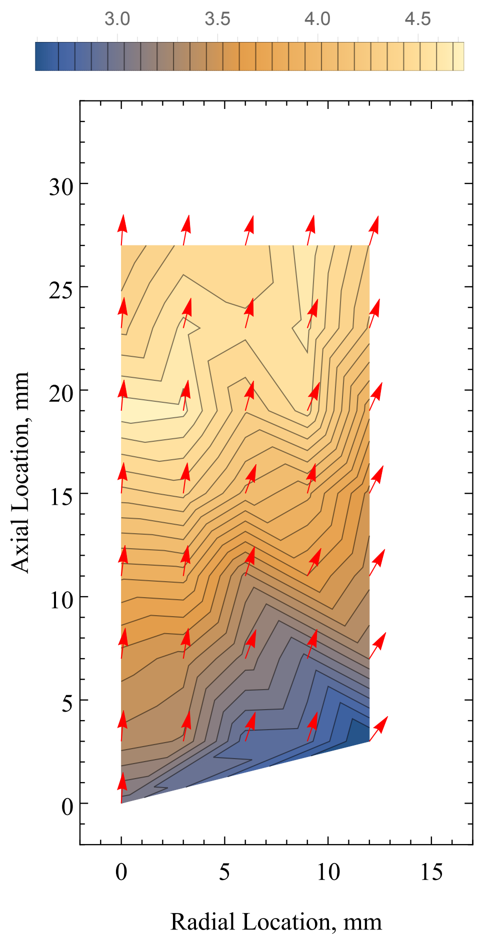

(a) Ion drift direction and speed (km/s). The vectors are normalized to their magnitude.

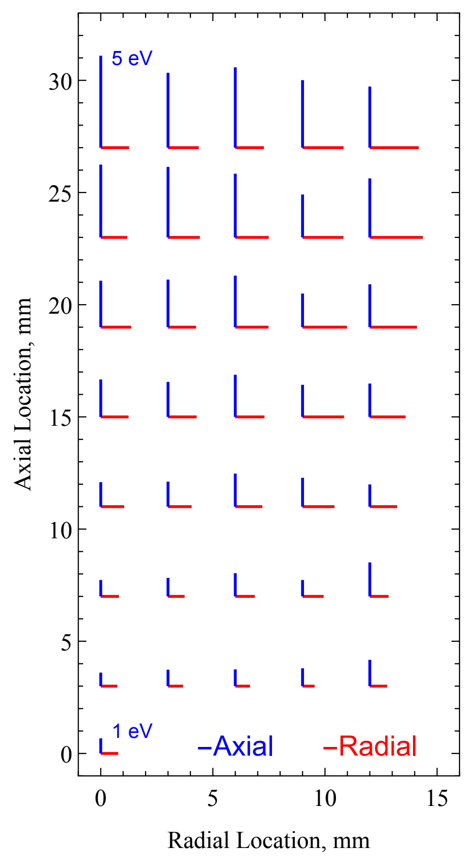

(b) Ion temperature along axial and radial projections of the IVDF. The length of each bar corresponds to the temperature magnitude.

Figure 7. Ion drift direction, speed, and temperature components.

Using the 1D temperatures measured from the two injection beams, the ion temperature anisotropy along the centerline is computed and shown in Fig. 8. Note that due to symmetry the plasma drift, ion acoustic wave vectors, and all gradients are assumed to be directed along the axis. Neglecting mechanisms that might cause the 2D IVDF to be skewed, we assume the 2D IVDF along the axis to consist of a bimodal Maxwellian with slow and fast populations along the axis with a single radial velocity distribution function. Therefore the anisotropy shown along the centerline can be used as an indication of that expected off-axis given that no magnetic field is present. Because the model used by McMahon[8] for correcting density estimates in a flowing plasma are for isotropic ion temperature distributions, this result indicates that more precise density estimates should incorporate a 2D IVDF as an input. Because of the possibility that IAW's are heating ions predominantly in the direction of propagation, it is not possible to use the measured IVDF's from this experiment to project the distribution along the direction of IAW propagation. This would require obtaining the 2D IVDF along several angles and applying a tomographic reconstruction technique, which was not possible with the current experimental configuration.

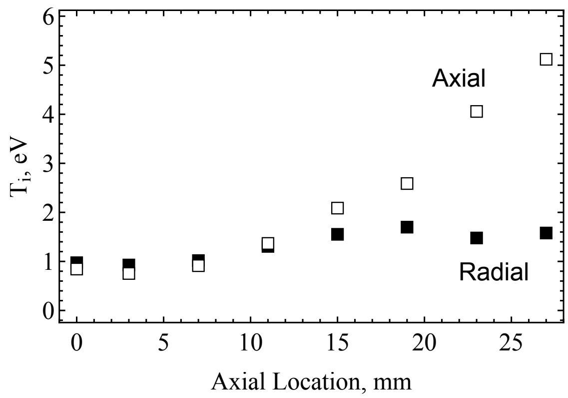

Figure 8. Axial and radial ion temperature components along the centerline.

C. Ion Acoustic Wave Measurements

The normalized wave vectors obtained using the vector sum of the orthogonally-measured phase velocity components, overlaid on a contour plot of the wave energy density (Eq. 3), are shown in Fig. 9(a). The domain was sampled with Δr=3 mm and Δz=2 mm. The locations of the wave vectors used to generate this correspond to the location of the corner probe shown in Fig. 2. The contour plot was generated using first order interpolation. The vectors for some locations are not shown due to the low signal-to-noise ratio in those regions. The wave energy grows with distance from the orifice and is strongest on the centerline, and the waves propagate outward from the orifice. Since the energy source for IAT is the electron drift, and the electrons carry the discharge current to the anode, it is reasonable for the waves to propagate outward from the orifice in the direction of the anode.

The wave vectors are also compared to the normalized ion drift vectors (for the fast population only) in Fig. 9(b), and it is found that the two are approximately collinear. As discussed in Sec. II, the wave energy is highest in the direction of the relative drift between the electrons and ions. Given this assumption, Fig. 9(b) indicates that the ions and electrons are drifting collinearly. This would be expected in a magnetic field-free ambipolar plasma, but not necessarily in the cathode plume because of the large (predominantly electron) current carried to the anode. It is possible that it is a coincidence that the vectors line up given that there is uncertainty in vector directions, probe effects could be significant, there is ion temperature anisotropy, and the fact that there are multiple ion populations. However, this observation warrants further investigation to see if it is possible that wave-particle effects in the direction of the acoustic waves is causing the ion velocity change. As mentioned in Sec. B, to establish a more direct correlation between IAT wave energy and ion heating, more information about the 2D IVDF is needed.

V. Conclusion

LIF and ion acoustic wave measurements were taken in the plume of a high current hollow cathode. Analysis of particle drifts found in this and previous experiments indicate that a more detailed accounting of drift effects is needed to improve the accuracy of the steady-state plasma properties and calculations derived from them. This is particularly the case for electron temperature which is linearly related to the ion acoustic wave energy. A preliminary analysis shows the ion distribution function along the the centerline is heated primarily in the axial direction, possibly by ion acoustic turbulence. The ion temperature anisotropy,

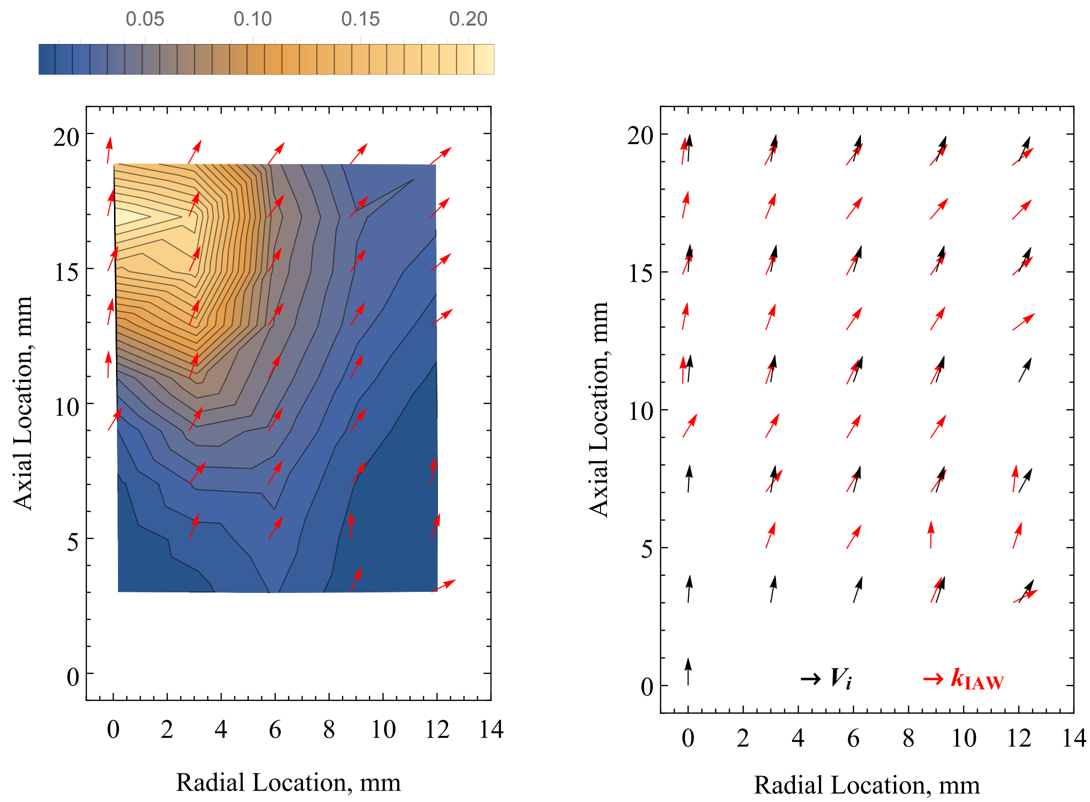

(a) Normalized ion acoustic wave vectors overlaid on IAT wave energy (eV).

(b) Ion acoustic wave and ion drift vectors.

Figure 9. Wave energy and drift properties.

if caused by ion acoustic turbulence, is expected to exist in the off-axis plume locations but cannot be confirmed without more LIF measurements. A bimodal ion velocity distribution function was observed with the axial LIF beam: the slow peak is believed to be caused by ion generation in the plume through ionization or charge-exchange collisions, whereas the acceleration of the fast ion population is unexplained. Wave energy and direction were calculated using measurements of the fluctuating ion saturation currents. It was found that the wave energy increased with distance downstream and was concentrated along the centerline. The ion acoustic waves were observed to propagate outward from the orifice in the direction of the drift of the fast ion population. Future analysis will compare the results presented here to other operating conditions to evaluate the effects that gas flow rate and discharge current have on the ion drift and temperature, and on the propagation of ion acoustic waves in the plumes of high power hollow cathodes.

Acknowledgments

The research described in this paper was carried out at the Jet Propulsion Laboratory, California Institute of Technology, under a contract with the National Aeronautics and Space Administration. It was also supported by the National Science Foundation Graduate Research Fellowship under Grant No. DGE-1144087, and the Air Force Office of Scientific Research under Grant No. FA9550-14-10317. The support of the joint NASA GRC and JPL development of HERMeS by NASA's Space Technology Mission Directorate through the Solar Electric Propulsion Technology Demonstration Mission (SEP TDM) project is gratefully acknowledged. The authors would also like to acknowledge Ray Swindlehurst and Nowell Niblitt for their assistance in running the experimental facility, Amine Elfhasi for preparing the diagnostics setup, Taylor Matlock for probe theory discussions, and Dan Goebel for his help on various aspects of hollow cathode research.

References

[1]Mikellides, I. G., Katz, I., Goebel, D. M., and Jameson, K. K., "Evidence of nonclassical plasma transport in hollow cathodes for electric propulsion," *Journal of Applied Physics*, Vol. 101, No. 6, 2007.

[2]Dodson, C. A., Perez-Grande, D., Jorns, B. A., Goebel, D. M., and Wirz, R. E., "Laser-induced Fluorescence Measurements of Energetic Ions in a 100-A LaB6 Hollow Cathode," *52nd AIAA/SAE/ASEE Joint Propulsion Conference*, 2016, pp. 1–17.

[3]Jorns, B. A., Lopez-Orgega, A., and Mikellides, I. G., "First-principles modeling of IAT-driven anomalous resistivity in hollow cathodes discharges I: Theory," *52nd AIAA/SAE/ASEE Joint Propulsion Conference*, 2016.

[4]Jorns, B. A., Dodson, C., Goebel, D. M., and Wirz, R., "Propagation of ion acoustic wave energy in the plume of a high-current LaB6 hollow cathode," *Physical Review E*, Vol. 96, No. 2, 2017, pp. 023208.

[5]Kadomtsev, B. B., *Plasma Turbulence*, Academic Press, New York, 1st ed., 1965.

[6]Jorns, B. A., Mikellides, I. G., and Goebel, D. M., "Ion acoustic turbulence in a 100-A LaB 6 hollow cathode," *Physical Review E*, Vol. 90, No. 6, 2014.

[7]Chen, F. F., "Langmuir probe diagnostics," *Mini-Course on Plasma Diagnostics, IEEE-ICOPS Meeting, Jeju, Korea*, 2003.

[8]McMahon, J. C., Xu, G. Z., and Laframboise, J. G., "The effect of ion drift on the sheath, presheath, and ion-current collection for cylinders in a collisionless plasma," *Physics of Plasmas*, Vol. 12, No. 6, 2005, pp. 1–11.

[9]Sheridan, T. E. and Goree, J., "Langmuir-probe characteristic in the presence of drifting electrons," *Physical Review E*, Vol. 50, No. 4, 1994, pp. 2991–2996.

[10]Stix, T., *Waves in Plasmas*, AIP-Press, New York, 1st ed., 1992.

[11]Beall, J. M., "Estimation of wavenumber and frequency spectra using fixed probe pairs," *Journal of Applied Physics*, Vol. 53, No. 6, 1982, pp. 3933.

[12]Manzella, D. H., "Stationary Plasma Thruster Ion Velocity Distribution," Tech. rep., 1994.

[13]Hargus, W. A. and Charles, C. S., "Near Exit Plane Velocity Field of a 200-Watt Hall Thruster," *Journal of Propulsion and Power*, Vol. 24, No. 1, Jan 2008, pp. 127–133.

[14]Chaplin, V. H., Conversano, R. W., Lobbia, R. B., Ortega, A., Mikellides, I. G., Hofer, R. R., and Jorns, B. A., "Laser-induced Fluorescence Measurements of the Acceleration Zone in the 12.5 kW HERMeS Hall Thruster," *35th International Electric Propulsion Conference*, 2017.